Journal of Mines, Metals and Fuels, *71(12C): 102-113; 2023. DOI: 10.18311/jmmf/2023/47272*

Print ISSN : 0022-2755

Journal of Mines, Metals and Fuels

Contents available at: *www.informaticsjournals.com/index.php/jmmf*

A Comprehensive Study on Molecular Geometry, HOMO-LUMO, and Global Reactivity Descriptors of Quinolin-2(1H)-One Substituted Coumarin Derivative: A Computational Approach

Ramani Sudha[1], D. Roopa[2], Misbhauddin Khan[3], Radha Rammohan Shanthanam[1], A. Anthony Seleen[4], Lohit Naik[5]*, Yin Yao[6], Yury Kapelyushin[7], Charles Mbohwa[8], and U. Mahaboob Pasha[1,8]

[1]*Presidency University, Bangalore - 560064, Karnataka, India; ramanisudhamohan@gmail.com*
[2]*Government First Grade College, Bannur, Mysore - 571101, Karnataka, India; roopadwar14@gmail.co*
[3]*Government College for Women, Kolar - 563101, Karnataka, India; drkhan1973@gmail.com*
[4]*Government First Grade College, KGF - 563122, Karnataka, India*
[5]*Christ University, Bangalore - 560026, Karnataka, India; Lohitishwar.naik@christuniversity.in*
[6]*Electron Microscope Unit, Mark Wainwright Analytical Centre, UNSW Sydney, Sydney, New South Wales, 2052, Australia*
[7]*Faculty of Materials Science and Metallurgy Engineering, South Ural State University (National Research University), Prospekt Lenina, 76, Chelyabinsk, Chelyabinsk Oblast - 454080, Russia*
[8]*College of Science Engineering and Technology, University of South Africa, Pretoria, South Africa*

Abstract

This research article presents Density Functional Theory (DFT) investigations on a 4-(2-(1H-imidazol-1-yl)-1-(2-oxo-2H-chromen-3-yl)ethoxy)quinolin-2(1H)-one (4HCQ). Employing DFT calculations, we explored various energy components of 4HCQ in its ground state, both in isolation and in diverse solvent environments, to examine solvent effects. Our analysis extends to the optimized geometry, Mulliken charge distribution in both ground and excited states, and the computed highest occupied molecular orbital, lowest unoccupied molecular orbital gap of 4HCQ in different mediums, allowing for the determination of solvation energy, ionization potential, electron affinity, chemical hardness, electron chemical potential, electronegativity and global electrophilicity. The density distribution analysis through total electron density and molecular electrostatic potential to understand the potential distribution over the molecule. Additionally, frontier molecular orbitals analysis was conducted. Overall, our study aims to elucidate the electronic, thermodynamic, and spectroscopic parameters of the coumarin derivative, considering solvent and solute-solvent interactions. The insights gained into the structural, electronic, and optical properties of this compound contribute to a deeper comprehension of its behavior in different mediums, with potential implications for exploring its optoelectronic application.

Keywords: *Coumarin Derivative, FMO, MESP, Mulliken, UV-Vis*

**Author for correspondence*

1.0 Introduction

The discovery of novel drug candidates continues to be a pivotal aspect of pharmaceutical and biochemical research, with a particular focus on improving therapeutic efficacy and minimizing adverse effects. Recently, 1-Aza-Coumarin-Linked Miconazole derivatives have attracted considerable attention not only for their pharmacological properties but also for their potential optoelectronic applications. Miconazole, a well-known antifungal agent, serves as the foundational scaffold for coupling with 1-Aza-Coumarin, which imparts additional functional properties. This hybrid molecule holds promise in addressing drug-resistant fungal infections and exploring new optoelectronic avenues[1-5].

The synthesis of 1-Aza-Coumarin-Linked Miconazole derivatives involves conjugating miconazole with 1-Aza-Coumarin through appropriate linker molecules. This strategic modification aims to enhance the bioactivity and optoelectronic properties of miconazole by leveraging the structural attributes of both moieties[6-8]. The incorporation of 1-Aza-Coumarin introduces functionalities such as antioxidant, anti-inflammatory, antimicrobial activities, and optoelectronic properties, complementing the antifungal characteristics of miconazole[9,10]. Moreover, the hybridization of these pharmacophores may lead to synergistic effects, potentially overcoming drug resistance mechanisms observed with conventional antifungal agents. The resulting derivatives exhibit improved solubility, bioavailability, targeted delivery, and enhanced optoelectronic properties, thereby optimizing therapeutic and optoelectronic outcomes while minimizing off-target effects. Furthermore, the structural diversity achievable through the modification of the linker and substitution patterns offers a wide array of derivatives with tailored properties for specific applications. Computational modelling and structure-activity relationship studies play a crucial role in elucidating the underlying molecular mechanisms and guiding the design of optimized derivatives with enhanced efficacy and optoelectronic performance[11-15].

In view of the above, 1-Aza-Coumarin-Linked Miconazole derivatives represent a promising class of compounds with multifaceted pharmacological and optoelectronic attributes. In light of the above discussion, the present work focuses on the compound, examining its photophysical and chemical properties through Density Functional Theory (DFT) analysis.

2.0 Analysis of Density Functional Theory

The 1-Aza-Coumarin-Linked Miconazole derivatives, namely 4-(2-(1H-imidazol-1-yl)-1-(2-oxo-2H-chromen-3-yl)ethoxy)quinolin-2(1H)-one (4HCQ) is selected from the literature[16] and the molecular structure of the 4HCQ was given in Figure 1.

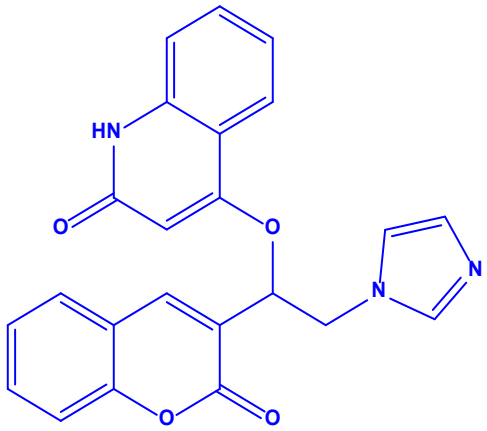


Figure 1. Molecular structure of the 4HCQ molecule.

The structural and theoretical analyses of 4HCQ were conducted using GaussView 5.0 and Gaussian 09 W software packages[17]. The optimization of 4HCQ geometry was initially performed via Density Functional Theory (DFT) employing the B3LYP functional and 6-311G basis set. Subsequently, various theoretical investigations were carried out, encompassing atomic charge distribution in the ground state, Time-Dependent DFT (TD-DFT) analysis in the excited state, thermodynamic properties, structural properties, and optical properties. The DFT method B3LYP/6-311G was utilized for these analyses. Additionally, frontier molecular orbital analysis of the molecule was conducted both in vacuum and in a liquid phase environment. This comprehensive approach enabled a thorough exploration of 4HCQ's electronic structure, thermodynamic behavior, and optical characteristics, shedding light on its potential applications and informing further research endeavors.

Thermodynamic parameters including Self-Consistent Field (SCF) energy, enthalpy, entropy, dipole moment, zero-point vibrational energy, heat capacity, and rotational constants were computed to elucidate 4HCQ's energetic and structural attributes. Furthermore, UV-Vis and emission spectroscopic analyses were performed on 4HCQ in various media, utilizing Time-Dependent Density Functional Theory (TDDFT) at the B3LYP/6-311G level. This provided insights into the molecule electronic transitions and oscillatory strengths under different environmental conditions. Moreover, the energy levels of the HOMO and LUMO were examined across different mediums, allowing for the assessment of key molecular properties such as ionization ability, electron affinity, chemical hardness, and electrophilic index. Additionally, Density Functional Theory (DFT) was employed to analyze the Total Electron Density (TED) surface mapping, Electrostatic Potential (ESP), and Molecular Electrostatic Potential (MEP), contour mapping of 4HCQ in both vacuum and solvent mediums, offering insights into its molecular interactions.

3.0 Results and Discussion

3.1 Structure and Geometric Properties

The structural design of 4HCQ was initially generated in GaussView-5 and subsequently optimized using Gaussian 09 software. The optimization process, conducted with the "opt" keyword, utilized the B3LYP functional and the 6-311G basis set[18]. Starting from standard parameters, the Gaussian program iteratively minimized the geometry to identify the configuration with the lowest energy, resembling the molecular structure at its energy minimum. The resulting optimized molecular geometries of 4HCQ are depicted in Figure 2, providing visual representation of the molecule's conformational characteristics.

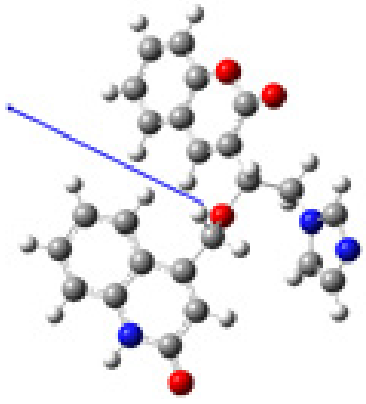


Figure 2. Optimised molecular geometry of the 4HCQ molecule.

The structural analysis of the molecule 4-(2-(1H-imidazol-1-yl)-1-(2-oxo-2H-chromen-3-yl) ethoxy)quinolin-2(1H)-one reveals detailed insights into its bond lengths, bond angles, and dihedral angles, as presented in Table 1. The carbon-hydrogen (C-H) bond lengths range from 1.082 Å to 1.097Å, indicating standard bonding. The carbon-carbon (C-C) bond lengths vary between 1.374 Å and 1.543 Å, encompassing both single and double bonds. The double bond length between atoms C1 and O31 measures 1.233 Å, typical of strong pi-bond interactions, while the single bond length between C1 and O30 is also noted as 1.233 Å, suggesting a possible typographical error or requiring further clarification. Carbon-nitrogen (C-N) bond lengths are reported as N14-C15 at 1.459 Å, N14-C16 at 1.382 Å, and C31-N49 at 1.395 Å, consistent with standard C-N single bonds.

The bond angle formed by atoms C1-O22-C22 is the largest at 122.61°, indicative of a near-trigonal planar configuration around the oxygen atom. The angle between atoms C18-C16-N14 is 105.13°, slightly larger than the typical tetrahedral angle, suggesting some strain or deviation from ideal sp3 hybridization. Dihedral angles within the benzene ring are smaller, reflecting its planar structure. Specific dihedral angles include C24-C25-C27-N14 at 176.09°, C25-O30-C45-C34 at 175.57°, H26-C25-C27-H29 at 179.88°, H28-C27-C25-O30 at 175.3°, and H47-C45-O30-C25 at 54.65°. These values indicate various degrees of torsional strain and conformational preferences within the molecule[19].

The Mulliken atomic charge distributions[20] of each atomic site in 4HCQ were investigated using DFT with the B3LYP/6-311G method in three different environments: vacuum, hexene, and dimethyl sulfoxide solvents (DMSO) which are useful for varies atomic and molecular fields. Table 2 presents the Mulliken charge distribution of each atom in 4HCQ different mediums, highlighting the solvent influences. Figures 3 and 4 were shows graphically illustrates of the variation in charge distribution across molecules. Notably, the atomic charges exhibited an increase with the polarity of

Table 1. Estimation of Bond length (Å), Bond angle (°) and dihedral angle of HCE using DFT/B3LYP/6-311G

Atoms	Bond length (Å)	Atoms	Bond Angle (°)	Atoms	Dihedral Angle (°)
1C-23O	1.233	C1-O22-C22	122.61	C24-C25-C27-N14	176.09
1C-22O	1.414	O22-C1-O23	112.23	C25-O30-C45-C34	175.57
6C-5H	1.097	C24-C25-C27	111.15	H26-C25-C27-H29	179.88
24C-25C	1.514	C25-C27-N14	112.79	H28-C27-C25-O30	175.31
25C-27C	1.543	C27-C25-O30	109.18	H47-C45-O3O-C25	54.65
27C-N14	1.459	C15-N14-C16	106.81		
N14-15C	1.382	N14-C15-N21	111.43		
15C-21N	1.328	C15-N21-C18	105.13		
21N-18C	1.396	N21-C18-C16	110.23		
18C-16C	1.374	C18-C16-N14	105.92		
16C-14N	1.394	O30-C45-C34	107.94		
25C-30O	1.459	N49-C31-O44	120.66		
30O-45C	1.471	C31-N49-C32	125.46		
45C-34C	1.506				
34C-35C	1.359				
31C-44O	1.252				
31C-49N	1.395				
49N-32C	1.388				
N49-C32	1.388				
N49-H50	1.010				
C37-H36	1.082				
C45-H47	1.094				

the solvent, with the highest values observed in DMSO. In vacuum, specific carbon and nitrogen atoms showed negative charges, suggesting donor characteristics, while others acted as acceptors. Transitioning to hexene, a slight increase in hydrogen and carbon atom charges was noted, along with a noticeable rise in the charge of nitrogen atoms compared to the vacuum. In DMSO, an overall elevation in atomic charges was observed across all atoms, indicating enhanced solvation effects. Additionally, a marginal increase in oxygen atom charge was evident with the shift from vacuum to hexene and further to DMSO. These insights into atomic charge distribution provide valuable information for understanding molecular interactions and the influence of solvents on 4HCQ's chemical behavior.

The results reveal distinct variations in atomic charges depending on the environment. In a vacuum, the atomic charges range from positive values on certain hydrogen

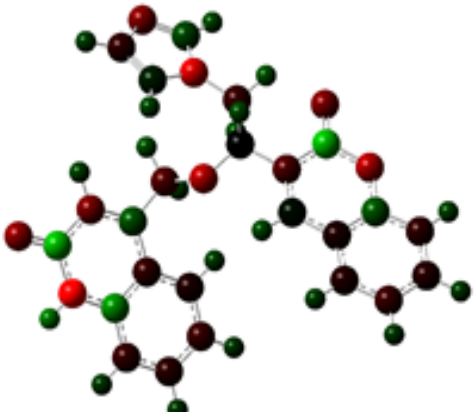


Figure 3. Mulliken charge distribution on the 4HCQ molecule.

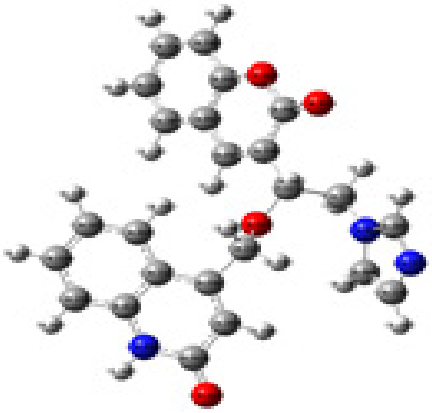


Figure 4. A statistical representation of Mulliken charge distribution on the 4HCQ molecule in the gas phase.

atoms, such as H50 with a charge of 0.528, to highly negative values on nitrogen and oxygen atoms, such as N48 with a charge of -0.812. The carbon atoms exhibit a wide range of charges, with the highest positive charge being on C1 (0.528) and the highest negative charge on C37 (-0.187). When the molecule is placed in hexane, a non-polar solvent, there is a general trend of increasing positive charges and decreasing negative charges compared to the vacuum environment. For instance, the charge on C1 increases from 0.528 in vacuum to 0.667 in hexane, and the charge on N48 decreases from -0.812 to -0.673. This shift indicates a redistribution of electron density due to the solvent effect, which typically reduces the extremity of charge values. In DMSO, a polar solvent, the charges further adjust, generally leading to an even greater polarization compared to hexane. The charge on C1 increases to 0.782, showing a significant positive shift, while the charge on N48 further decreases to -0.558. Polar solvents like DMSO tend to enhance the separation of charges due to their high dielectric constant, which stabilizes charges. Specific observations include hydrogen atoms such as H5, H8, and H50 exhibiting increasing positive charges from vacuum to hexane to DMSO, reflecting their increased electron deficiency in more polar environments. Carbon atoms like C1, C2, and C31 show a trend of increasing positive charge, indicating a higher electron withdrawing effect of the environment. Conversely, some carbon atoms such as C6 and C27 move from slightly negative or neutral in vacuum to slightly positive in solvents. Nitrogen atoms (N14, N21, N48) and oxygen atoms (O22, O23, O30) generally become less negative as the polarity of the solvent increases, which aligns with their tendency to stabilize in polar environments due to their electronegativity. The Mulliken charge analysis demonstrates that the electronic distribution within 4-(2-(1H-imidazol-1-yl)-1-(2-oxo-2H-chromen-3-yl)ethoxy)quinolin-2(1H)-one is significantly influenced by the surrounding medium. The transition from vacuum to hexane to DMSO shows a clear trend of increased polarization, with atomic charges becoming more extreme in polar solvents. This behavior is crucial for understanding the molecule's reactivity, stability, and interaction with other molecules in different environments.

The thermodynamic parameters serve as pivotal indicators in understanding chemical processes. Utilizing Density Functional Theory (DFT), we investigated various statistical thermodynamic properties of 4HCQ at a temperature of 298.15 K and 1atm pressure. The DFT/B3LYP/6-311G method facilitated the determination of translational, rotational, vibrational, total, and nuclear repulsion energies, as well as zero-point vibrational energy and other statistical thermodynamic parameters such as entropy (S), rotational constants, molecular capacity at constant volume, and dipole moment. These findings, outlined in Table 3, provide essential insights for further exploration of 4HCQ's molecular behavior and pave the way for comprehensive studies on this compound[21].

The calculated thermodynamic parameters for the molecule 4-(2-(1H-imidazol-1-yl)-1-(2-oxo-2H-chromen-3-yl)ethoxy)quinolin-2(1H)-one using DFT with the B3LYP/6-311G (d, p) basis set offer valuable

Table 2. Mulliken atomic charges by DFT/ B3LYP/6-311G in vacuum and solvent medium

Atom label	Vacuum	Hexene	DMSO
1C	0.528	0.667	0.782
2C	0.301	0.44	0.555
3C	-0.176	-0.037	0.078
4C	0.059	0.198	0.313
5H	0.185	0.324	0.439
6C	-0.153	-0.014	0.101
7C	-0.078	0.061	0.176
8H	0.199	0.338	0.453
9C	-0.181	-0.042	0.073
10C	-0.097	0.042	0.157
11C	0.176	0.315	0.43
12H	0.163	0.302	0.417
13H	0.166	0.305	0.42
14N	-0.53	-0.391	-0.276
15C	-0.077	0.062	0.177
16C	0.085	0.224	0.339
17H	0.232	0.371	0.486
18C	-0.102	0.037	0.152
19H	0.209	0.348	0.463
20H	0.197	0.336	0.451
21N	-0.292	-0.153	-0.038
22O	-0.401	-0.262	-0.147
23O	-0.397	-0.258	-0.143
24C	-0.261	-0.122	-0.007
25C	-0.009	0.13	0.245
26H	0.2	0.339	0.454
27C	-0.154	-0.015	0.1
28H	0.249	0.388	0.503
29H	0.136	0.275	0.39
30O	-0.486	-0.347	-0.232
31C	0.512	0.651	0.766
32C	0.444	0.583	0.698
33C	-0.216	-0.077	0.038
34C	0.238	0.377	0.492
35C	-0.313	-0.174	-0.059

36H	0.167	0.306	0.421
37C	-0.187	-0.048	0.067
38C	-0.038	0.101	0.216
39H	0.183	0.322	0.437
40C	-0.181	-0.042	0.073
41C	-0.106	0.033	0.148
42H	0.177	0.316	0.431
43H	0.157	0.296	0.411
44O	-0.44	-0.301	-0.186
45C	-0.272	-0.133	-0.018
46H	0.299	0.438	0.553
47H	0.186	0.325	0.44
47H	0.155	0.294	0.409
48H	-0.812	-0.673	-0.558
49N	0.357	0.496	0.611
50H	0.528	0.667	0.782

insights into its energetic and structural properties. The translational and rotational energies are both 0.695 kcal mol^{-1}, reflecting the kinetic energy associated with the molecule's centre of mass motion and rotational motion around its principal axes, respectively. The vibrational energy is significantly higher at 91.193 kcal mol^{-1}, representing the energy stored in the molecule's vibrational modes. Summing these components, the total energy amounts to 92.583 kcal mol^{-1}, providing a comprehensive view of the molecule's overall kinetic energy.

The nuclear repulsion energy is calculated to be 1298 Hartrees, indicating the electrostatic repulsion between the positively charged nuclei within the molecule, which is a critical factor in determining the molecule's overall stability and conformation. The Zero-Point Vibrational Energy (ZPVE) is 93.219 kcal mol^{-1}, reflecting the energy present in the molecule at absolute zero temperature due to quantum mechanical vibrations of atoms, providing a baseline energy understanding of the molecule.

The entropy of the molecule is 109.210 cal/mol-K, a measure of the disorder or randomness in the system, with higher entropy indicating greater molecular disorder at a given temperature. The molecular heat capacity at constant volume (C_v) is 3.788 cal/mol-K, with contributions from translational (1.214 cal/mol-K), rotational (33.154 cal/mol-K), and vibrational (47.123 cal/mol-K) modes. These values illustrate how the molecule's energy changes with temperature, reflecting its ability to store thermal energy.

The rotational constants are 1.190 GHz (A), 0.125 GHz (B), and 0.149 GHz (C), describing the molecule's rotation around its principal axes and providing insights into its rotational spectrum and moments of inertia. The dipole moment is 10.661 Debye, indicating significant polarity and affecting the molecule's interactions with electric fields and other dipolar molecules. Thermodynamic parameters indicate that 4-(2-(1H-imidazol-1-yl)-1-(2-oxo-2H-chromen-3-yl)ethoxy)quinolin-2(1H)-one has substantial vibrational energy compared to translational and rotational energies, highlighting the importance of vibrational modes in its thermodynamic behavior. The high nuclear repulsion energy suggests strong electrostatic interactions within the molecule. The entropy value suggests moderate molecular disorder, while the heat capacity values indicate the molecule's ability to absorb heat. The rotational constants provide insights into the molecule's rotational characteristics, and the dipole moment indicates significant molecular polarity, which will affect its interactions and solubility in various environments. Overall, these parameters

Table 3. Calculated thermodynamic parameters of 4HCQ with DFT theory using the B3LYP/6-311G (d, p) basis set

Parameters	Values
Energy	
Translational (kcal mol^{-1})	0.695
Rotational (kcal mol^{-1})	0.695
Vibrational (kcal mol^{-1})	91.193
Total	92.583
Nuclear repulsion energy (Hartree's)	1298
Zero-point vibrational energy (kcal mol^{-1})	93.219
Entropy, S (Cal/Mol-Kelvin)	109.210
Molecular capacity of constant volume (cal mol^{-1} k^{-1})	3.788
Translational	1.214
Rotational	33.154
Vibrational	47.123
Rotational constants (GHz)	81.491
A	1.190
B	0.125
C	0.149
Dipole moment (D)	10.661

provide a comprehensive understanding of the molecule's energetic, structural, and thermodynamic properties, essential for predicting its behavior in different conditions and potential applications.

3.2 Frontier Molecular Orbitals (FMO) and Quantum Chemical Simulation

The FMO enables recognition of the electron charge transfer between the donor and acceptor groups via the π-conjugate system. The HOMO (electron-donating) is directly associated with the ionization potential, while the LUMO (electron-accepting) is associated with the electron affinity of the compound. Plotting the FMO provides deeper insights into the nature of the chemical structure and reactions of the molecule[9,22]. HOMO, HOMO-1, and HOMO-2 are orbitals that exhibit π-bonding symmetry, while LUMO, LUMO+1, and LUMO+2 are molecular orbitals that show π* antibonding symmetry. Figure 5 presents a 3D representation of the frontier molecular orbitals in different media using the DFT method with the B3LYP functional and the 6-311G basis set, where the greenish area indicates the positive region and the reddish area represents the negative region of the molecular orbital.

The energy gap (E_g) has been analyzed using equation (1) provided below, which gives the energy gap (E_g) between the HOMO and LUMO. The E_g in the DMSO medium shows the largest energy gap of 4.205 eV, the energy gap between HOMO-1 and LUMO+1 is 6.073 eV, and the E_g between HOMO+2 and LUMO-2 is 6.540 eV.

The global chemical reactivity descriptors (GCRD) for the molecule 4-(2-(1H-imidazol-1-yl)-1-(2-oxo-2H-chromen-3-yl)ethoxy)quinolin-2(1H)-one provide critical insights into its stability and reactivity and the values are given in Table 4. The chemical hardness (η) of the molecule is 1.926 eV, indicating a relatively stable structure with resistance to changes in electron distribution. High chemical hardness typically correlates with greater stability and lower reactivity. The molecule's electronegativity (χ) is 4.544 eV, suggesting a strong tendency to attract electrons, which impacts its reactivity and interactions with other species.

The chemical potential (μ) is -4.544 eV, reflecting the molecule's tendency to accept electrons rather than donate them, which aligns with its high electronegativity. The chemical softness (S) of 0.260 eV^{-1} indicates moderate reactivity, as softer molecules are more polarizable and reactive. This value suggests that while the molecule can participate in chemical reactions, it is not highly reactive.

The electrophilicity index (ω) is 5.361eV, quantifying the molecule's ability to accept electrons. A higher electrophilicity index suggests the molecule is a strong electrophile, readily accepting electrons in reactions.

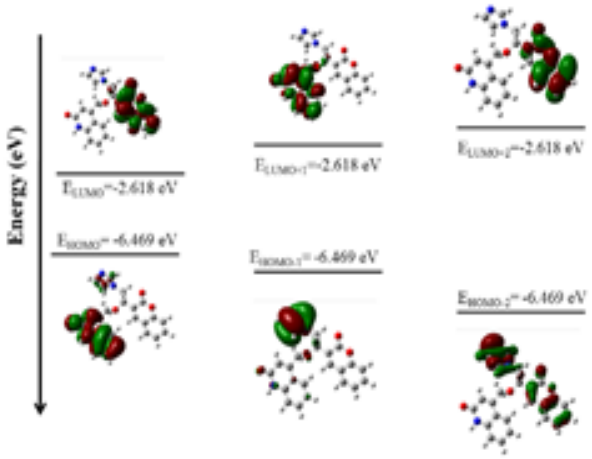


Figure 5. 3D representation of frontier molecular orbital of 4HCQ in DMSO using the DFT method.

The Ionization Potential (IP) of 6.469 eV and the Electron Affinity (EA) of 2.618 eV further support these findings. The ionization potential indicates the energy required to remove an electron from the molecule, with a higher value signifying greater stability against electron loss. The electron affinity reflects the energy change when the molecule gains an electron, with a higher value indicating a greater tendency to accept electrons.

The GCRD parameters suggest that 4-(2-(1H-imidazol-1-yl)-1-(2-oxo-2H-chromen-3-yl) ethoxy)quinolin-2(1H)-one is a relatively stable molecule with moderate reactivity. Its high electronegativity and negative chemical potential indicate a strong tendency to attract and accept electrons, making it an effective electrophile. The moderate chemical softness and significant electrophilicity index confirm its ability to participate in chemical reactions, particularly those where it acts as an electron acceptor. These properties are essential for understanding the molecule's behavior in various chemical environments and potential applications.

3.3 Electrostatic Potential (ESP), Total Electron Density (TED) and Molecular Electrostatic Potential (MESP) Studies

Three-dimensional mappings of electrostatic potential, total electron density and molecular electrostatic potential were generated using DFT theory with the B3LYP functional and 6-311+G (d,p) basic set. These mappings of 4HCQ structure were analysed through surface contouring in Gaussian-09W[23].

3.3.1 ESP of 4HCQ Molecule

Electrostatic Potential (ESP) illustrates the interaction energy between the molecule's electrons and point positive charges near nuclei. Figure 6 displays the ESP mapping of the 4HCQ molecule, indicating energy ranging from -0.349 eV to 0.349 eV in vacuum and from -0.288 eV to 0.288 eV in DMSO solvent. Notably, sites O30 and O31 exhibit the most negative potential values of -0.312 eV and -0.303 eV, respectively, in vacuum and these areas are highlighted in red. Additionally, the region encompassing 27N and 13N shows, the potential values of 0.121 eV and 0.111 eV (yellow) in vacuum

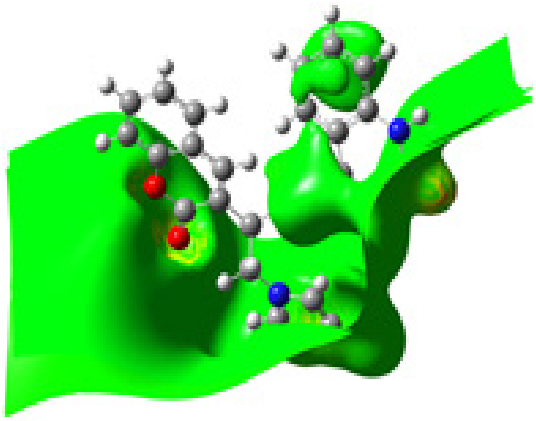


Figure 6. Electrostatic potential mapping of 4HCQ molecule in vacuum.

Table 4. Global electrochemical reactivity descriptor parameter for 4HCQ molecule

E_{HOMO} (eV)	E_{LUMO} (eV)	ΔE (eV)	IP (eV)	EA (eV)	h (eV)	c (eV)	μ (eV)	s (eV^{-1})	ω (eV)
−6.469	-2.618	3.851	6.469	2.618	1.926	4.544	−4.544	0.260	5.361

3.3.2 TED of 4HCQ Molecule

Density functional theory provides a theoretical framework to estimate this Total Electron Density (TED). Electron density mapping uses in analysing the molecule's shape, charge, and delocalization, offering insights into its chemical reactivity. Figure 7 illustrates the TED mapping of 4HCQ in vacuum, indicating electron densities of ± 4.031x10^{-4} Hartrees in vacuum. The electron density shows, a uniform distribution across the molecule's surface. These results help in understanding various properties of a system, such as chemical bonding, interactions and other important electronic properties.

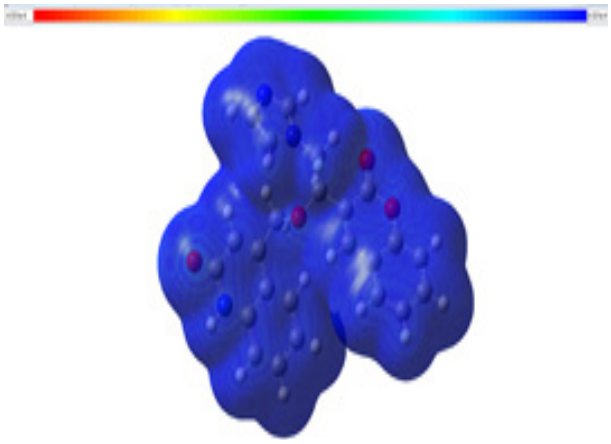


Figure 7. Total electron density mapping of 4HCQ molecule in vacuum.

3.3.3 MEP of 4HCQ Molecule

The molecular Electrostatic Potential (MESP) mapping, conducted using DFT/B3LYP/6-611G in various solvents, depicts potential distribution can be observed by colour code. Figure 8 presents the MESP mapping of 4HCQ in vacuum and DMSO, displaying contour values ranging from -7.158 eV to 7.158 eV in vacuum. The red regions, primarily surrounding 23O 22O and 44O, signify lower energy levels, making these atoms susceptible to nucleophilic attacks as electron acceptors. Conversely, the methyl group attached to carbon atom 20 C, 49N displays maximum positive charge (blue region), rendering them susceptible to electrophilic attacks as electron donors. Yellow colour around 14N

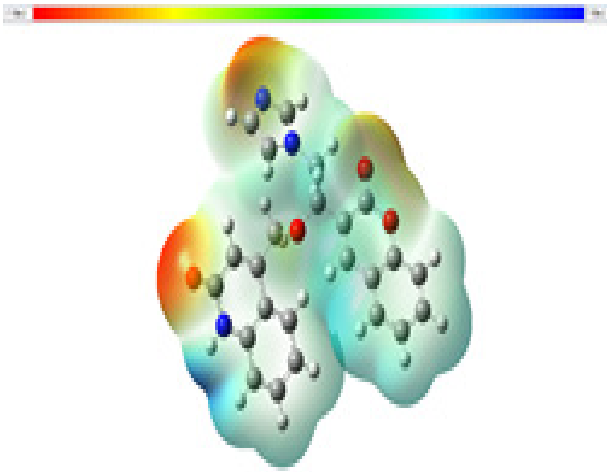


Figure 8. Molecular electrostatic potential mapping of 4HCQ molecule in vacuum.

and 21N represents nucleophilic sites. Neutral (green) region is widespread across the molecule, particularly on benzene ring structures and certain carbon atoms. Positive charge (light blue) is observed at the position of hydrogen indicating its role as an electron-donator[24].

4.0 Conclusion

This study has successfully employed a computational methodology integrating Density Functional Theory (DFT) and Time-Dependent Density Functional Theory (TD-DFT) to investigate the properties of the 4HCQ molecule towards photophysical and varies biological importance. The analysis of its geometry revealed critical structural features impacting orbital overlap and charge transfer absorption, emphasizing the significance of precise distances and angles. Further, the investigation of Frontier Molecular Orbital (FMO) energy gaps provided valuable insights into the compound chemical reactivity and stability. Notably, a lower FMO energy gap indicates heightened chemical reactivity and reduced kinetic stability, characterizing the molecule as 'soft'. Overall, this thorough theoretical analysis of the 4HCQ molecule contributes significantly to advancing our understanding of its behavior in various environments, thereby facilitating the exploration of its potential biological properties.

5.0 Reference

1. Prabhala P, Sutar SM, Manjunatha MR, Pawashe GM, Gupta VK, Naik L, Kalkhambkar RG. Synthesis, *in vitro* and theoretical studies on newly synthesized deep blue emitting 4-(p-methylphenylsulfonyl-5-aryl/alkyl) oxazole analogues for biological and optoelectronic applications. J Mol Liq. 2022; 360:119520. https://doi.org/10.1016/j.molliq.2022.119520
2. El Azab IH, Thabet HK, Almotairi SA, Saleh MGA, Mogharbel RT, Mahmoud SA, Al-Hossainy AF. Synthesis of a novel coumarin heterocyclic derivative and fabrication of hybrid nanocomposite thin film with $CoOFe_2O_4$ for optoelectronic applications. J Mol Struct. 2021; 1241:130640. https://doi.org/10.1016/j.molstruc.2021.130640
3. El-Mahalawy AM, Abdou MM, Wassel AR. Physical and optoelectronic characteristics of novel low-cost synthesized coumarin dye-based metal-free thin films for light sensing applications. Mater Sci Semicond Process. 2022; 137:106225. https://doi.org/10.1016/j.mssp.2021.106225
4. Arunkumar A, Shanavas S, Acevedo R, Anbarasan PM. Quantum chemical investigation of modified coumarin-based organic efficient sensitizers for optoelectronic applications. Eur Phys J D. 2020; 74:1-8. https://doi.org/10.1140/epjd/e2019-100246-9
5. Ebied MS, Dongol M, Ibrahim M, Nassary M, Elnobi S, Abuelwafa AA. Structural and optical properties of nanocrystalline 3-(2-benzothiazolyl)-7-(diethylamino) coumarin (C6) thin films for optoelectronic application. J Electron Mater. 2022; 51(10):5770-82. https://doi.org/10.1007/s11664-022-09792-4
6. Vuai SA, Khalfan MS, Babu NS. DFT and TD-DFT studies for optoelectronic properties of coumarin based donor-π-acceptor (D-π-A) dyes: applications in dye-sensitized solar cells (DSSCs). Heliyon. 2021; 7(11). https://doi.org/10.1016/j.heliyon.2021.e08339
7. Dayananda BS, Sarojini BK. Stoke's shift and quantum efficiency enhancement in fluorescent coumarin aldehyde (HMCA) dye-conjugated chitosan matrix for optoelectronic applications. Dyes Pigments. 2024; 223:111936. https://doi.org/10.1016/j.dyepig.2024.111936
8. Altınışık S, Özdemir M, Kortun A, Zorlu Y, Yalçın B, Köksoy B, Koyuncu S. Symmetrical and asymmetrical thiophene-coumarin-based organic semiconductors. ACS Omega. 2023; 9(3):3305-3316. https://doi.org/10.1021/acsomega.3c05602
9. El-adly A, Shabana I. Antimicrobial activity of green silver nanoparticles against fluconazole-resistant Candida albicans in animal model. Egypt J Bot. 2018; 58(1):119-32. https://doi.org/10.21608/ejbo.2018.1292.1110
10. Saha M, McDaniel JK, Zheng XL. Thrombotic thrombocytopenic purpura: pathogenesis, diagnosis and potential novel therapeutics. J Thromb Haemost. 2017; 15(10):1889-900. https://doi.org/10.1111/jth.13764
11. Kashyap PL, Xiang X, Heiden P. Chitosan nanoparticle-based delivery systems for sustainable agriculture. Int J Biol Macromol. 2015; 77:36-51. https://doi.org/10.1016/j.ijbiomac.2015.02.039
12. Gedeck P, Kramer C, Ertl P. Computational analysis of structure-activity relationships. Prog Med Chem. 2010; 49:113-60. https://doi.org/10.1016/S0079-6468(10)49004-9
13. Piir G, Kahn I, García-Sosa AT, Sild S, Ahte P, Maran U. Best practices for QSAR model reporting: physical and chemical properties, ecotoxicity, environmental fate, human health, and toxicokinetics endpoints. Environ Health Perspect. 2018; 126(12):126001. https://doi.org/10.1289/EHP3264
14. Taboureau O, Baell JB, Fernández-Recio J, Villoutreix BO. Established and emerging trends in computational drug discovery in the structural genomics era. Chem Biol. 2012; 19(1):29-41. https://doi.org/10.1016/j.chembiol.2011.12.007
15. Miteva MA, Villoutreix BO. Computational biology and chemistry in MTi: emphasis on the prediction of some ADMET properties. Mol Inform. 2017; 36(10):1700008. https://doi.org/10.1002/minf.201700008
16. Savanur HM, Pawashe GM, Kim KM, Kalkhambkar RG. Synthesis and molecular modelling studies of coumarin- and 1-aza-coumarin-linked miconazole analogues and their antifungal activity. ChemSelect. 2018; 3(33):9648-53. https://doi.org/10.1002/slct.201801408
17. Frisch MJ, Trucks GW, Schlegel HB, Scuseria GE, Robb MA, Cheeseman JR, *et al.* Gaussian-09, Revision B.01, Gaussian, Inc. Wallingford, CT; 2010.
18. Raghavachari K, Becke AD. Density functional thermochemistry. III. The role of exact exchange. J Chem Phys. 2000; 98. https://doi.org/10.1007/978-3-662-10421-7_60
19. Shirley WA, Hoffmann R, Mastryukov VS. An approach to understanding bond length/bond angle relationships. J Phys Chem. 1995; 99(12):4025-33. https://doi.org/10.1021/j100012a024
20. Tsuzuki S, Uchimaru T, Tanabe K, Yliniemela A. Comparison of atomic charge distributions obtained from different procedures: basis set and electron correlation effects. J Mol Struct Theochem. 1996; 365(2-3):81-8. https://doi.org/10.1016/0166-1280(96)04500-9

21. Petrushenko IK. Physical adsorption of N-containing heterocycles on hexagonal boron nitride: DFT-D3 study. J Nano Electron Phys. 2018; 10(2). https://doi.org/10.21272/jnep.10(2).02010
22. Zara Z, Iqbal J, Ayub K, Irfan M, Mahmood A, Khera RA, Eliasson B. A comparative study of DFT calculated and experimental UV/Visible spectra for thirty carboline and carbazole-based compounds. J Mol Struct. 2017; 1149:282-98. https://doi.org/10.1016/j.molstruc.2017.07.093
23. Nogueira JJ, González L. Computational photophysics in the presence of an environment. Annu Rev Phys Chem. 2018; 69:473-97. https://doi.org/10.1146/annurev-physchem-050317-021013
24. Tichnell CR, Shultz DA, Popescu CV, Sokirniy I, Boyle PD. Synthesis, characterization, and photophysical studies of an iron (III) catecholate-nitronylnitroxide spin-crossover complex. Inorg Chem. 2015; 54(9):4466-74. https://doi.org/10.1021/acs.inorgchem.5b00298